University of Groningen

Modeling the characteristics of spontaneous otoacoustic emissions in lizards

Wit, Hero P.; Manley, Geoffrey A.; van Dijk, P.

IMPORTANT NOTE: You are advised to consult the publisher's version (publisher's PDF) if you wish to cite from it. Please check the document version below.

Document Version
Publisher's PDF, also known as Version of record

Publication date:
2020

Link to publication in University of Groningen/UMCG research database

Modeling the characteristics of spontaneous otoacoustic emissions in lizards

Hero P. Wit [a, b, *], Geoffrey A. Manley [c], P. van Dijk [a, b]

[a] University of Groningen, University Medical Center Groningen, Department of Otorhinolaryngology/Head and Neck Surgery, Groningen, the Netherlands
[b] University of Groningen, Graduate School of Medical Sciences (Research School of Behavioral and Cognitive Neurosciences), Groningen, the Netherlands
[c] Cochlear and Auditory Brainstem Physiology, Department of Neuroscience, School of Medicine and Health Sciences, Cluster of Excellence "Hearing4all", Research Center Neuroscience, Carl von Ossietzky University Oldenburg, 26129, Oldenburg, Germany

ARTICLE INFO

ABSTRACT

Lizard auditory papillae have proven to be an attractive object for modelling the production of spontaneous otoacoustic emissions (SOAE). Here we use an established model (Vilfan and Duke, 2008) and extend it by exploring the effect of varying the number of oscillating elements, the strength of the parameters that describe the coupling between oscillators, the strength of the oscillators, and additive noise. The most remarkable result is that the actual number of oscillating elements hardly influences the spectral pattern, explaining why spectra from very different papillar dimensions are similar. Furthermore, the spacing between spectral peaks primarily depends on the reactive coupling between the oscillator elements. This is consistent with observed differences between lizard species with respect to tectorial covering of hair cells and SOAE peak spacings. Thus, the model provides a basic understanding of the variation in SOAE properties across lizard species.

1. Introduction

Among tetrapod vertebrates, the lizards display great structural variation in their hearing organs (Miller, 1966; Wever, 1978). Uniquely, lizard auditory papillae have at least two different populations of sensory hair cells, the papillae vary up to five times in length and up to 40 times in the number of hair cells. In addition, there are numerous variations in the structure such as the presence or absence of tectorial material covering the sensory cells. This group of vertebrates thus provides science with a wide range of natural experiments for studying the influence of structure on function (Manley, 2002, 2011; Manley and Köppl, 2008).

In all tetrapod groups studied so far, the auditory organs provide clear evidence of the presence of at least one active process. Active processes are those mechanisms that, at low sound levels, induce larger micromechanical responses of the sensory cells to stimuli than would be produced passively. Such active processes can be identified by a number of signature characteristics (Hudspeth, 1997; Manley, 2001). One manifestation of the active process is the spontaneous production of mechanical energy by the auditory organs in the complete absence of any external stimuli. This spontaneously produced vibratory energy is bundled at particular frequencies and some of it is emitted through the middle ear into the outside world. This portion of the energy can thus be measured near the eardrum by using appropriately sensitive microphone systems. These emitted signals are known as spontaneous otoacoustic emissions (SOAEs).

Using such measurement techniques, the influence of external factors on SOAEs, such as temperature, but also of externally applied sounds, can be studied (e.g., Köppl and Manley, 1994; Manley and Köppl, 1994). Such experiments have provided a great deal of information on the processes involved in the production and patterning of spontaneous otoacoustic emissions, especially in non-mammals (Manley and van Dijk, 2008). In lizards, which are unusually robust producers of SOAEs, there is strong evidence that the active process is contained within the hair cell's stereovillar bundle (Manley et al., 2001) and is intimately associated with the transduction process (Köppl, 1995; Hudspeth, 1997).

In many ways, however, the spectra of SOAEs from all amniote groups (mammals, birds, "reptiles") resemble each other far more than would be expected from the highly diverse dimensions and anatomical variations among and between these lineages. It is a striking fact that both avian and mammalian species rarely produce

* Corresponding author. University of Groningen, University Medical Center Groningen, Department of Otorhinolaryngology/Head and Neck Surgery, Groningen, the Netherlands.
E-mail address: hero.wit@ziggo.nl (H.P. Wit).

SOAEs, being so far only consistently found in the barn owl (Taschenberger and Manley, 1997) and in humans (e.g. Burns, 2009). While it is not yet clear why this is, the difference to lizard species is likely to be associated with the thick, continuous tectorial membranes of birds and mammals that perhaps produce a coupling of oscillators that is too strong to permit their local (or localised) spontaneous oscillation. Lizards, in contrast, show very different types of tectorial covering, including its absence.

From these observations arises the important question as to the origin of spectral patterns - since all hair cells have an active mechanism, why do we not simply measure a kind of "white noise" being emitted from the ear? Why are there clear and specific frequencies at which more sound energy is emitted? The patterns we see are presumably the result of a common mechanism underlying SOAE generation that results in interactions among the emitted vibratory energy within the hearing organ and the surrounding fluids. Vibratory activity from some groups of cells interacts in such a way that the energy can sum together into a steady tonal emission. This is the result of "phase coherence", i.e., the phases of the emitted signals are sufficiently coordinated as to only interact positively with each other and create a sustained emission (Bergevin et al., 2015a). Within the inner ear, sound energy emitted from different cells of a given frequency range that attain phase coherence will produce a more or less large spectral peak at that frequency. This condition is generally achieved for many arrays of cells that tend to have a characteristic frequency spacing, depending on the coupling conditions that prevail in different types of papillae (Shera and Guinan, 2003; Bergevin et al., 2015a,b), but also in individual ears. Thus we observe not only specific spectral patterns in different groups of vertebrates, but also individual, ear-specific spectra that are generally very stable over time (e.g., Burns, 2009). To some extent, the patterning of the spectra of SOAEs in lizards, i.e., the number and the frequencies of SOAE peak amplitudes, correlates with the specific anatomy of the auditory hearing organ, the auditory papilla. In particular, in the papillae of lizard families in which there is a thick and continuous tectorial membrane, and thus perhaps a strong coupling between groups of hair cells, SOAEs tend to be few but large in sound amplitude - sometimes more than 20 dB above the noise level. The opposite is true in species in which the tectorial coupling between hair cells is weaker or absent (Manley, 1997). Thus in lizard auditory papillae, the coupling of hair cells is one factor that influences spectral patterns.

These general features of SOAE spectra are now reasonably well understood. Previous models of SOAE spectral patterns, which were often based on the anatomy and SOAE spectra typical of certain species, producing fairly realistic spectra by using elastic coupling of oscillators and random variance in the strength of their output (Gelfand et al., 2010; Vilfan and Duke, 2008; Wit et al., 2012). The addition of external tones, by synchronising individual oscillator contributions at and near their own frequency, produced both loss of amplitude of peaks and changes in their frequency as the components of each cluster were affected. These models have, however, failed to reproduce important aspects of SOAE. In particular, the spectral peaks in previous models of lizard papillae were far too narrow in bandwidth and had uncharacteristic spacing. In addition, previous models have not addressed the fact that similar spectra with the same number of spectral peaks can be measured from auditory papillae that differ greatly in the number of hair cells (up to 40-fold) and thus in their physical size. Also not well explained is the variability of SOAE spectra in a single lizard species. For SOAE generation in human ears Fruth et al. (2014) provided an explanation by incorporating weak spatial disorder.

The work described here is an attempt to examine in more detail the factors responsible for (a) the characteristic spacing of spectral peaks, for (b) the bandwidth of these peaks, for (c) the frequent presence of spectral "plateaus" (a kind of raised noise floor over a certain frequency range), but also (d) to study the origin of similar spectra in species with very different sizes of papilla, and (e) the variability of spectra within a single species.

2. The model

The model is that of Vilfan and Duke (2008), who show that the properties of individual oscillators in a one-dimensional oscillator array, when clustered into "frequency plateaus" (Ermentrout and Kopell, 1984; Osipov and Sushchik, 1998; Daido, 1999), are comparable with published properties of SOAEs in the bobtail lizard. The model consists of a chain of n oscillators, in which each oscillator is coupled to its neighbours, and x_j and $\dot{x}_j$ are displacement and velocity of the jth oscillator respectively. If x_j and $\dot{x}_j$ are combined in the complex notation $z_j = x_j - \frac{1}{\omega_j} i \dot{x}_j$, the differential equation to be solved for the jth oscillator ($j = 1, 2, ..., n$) is:

$$\dot{z}_j = (i\omega_j + \varepsilon_j)z_j + (d_R + id_I)(z_{j-1} - 2z_j + z_{j+1}) - b_j |z_j|^2 z_j \qquad (1)$$

In equation (1) ω_j is the natural frequency of oscillator j (the frequency with which it will oscillate if it is not coupled to its neighbours); ε_j is a measure of the effective damping, being positive for an active oscillator and negative for a passive (damped) oscillator; d_R and d_I are dissipative and reactive coupling constants respectively; b_j describes the intrinsic nonlinearity of the oscillators and is necessary to preserve finite amplitude. The variables z_{j-1} and z_{j+1} reflect the interaction of an oscillator with its two neighbours. For the first oscillator of the chain ($j = 1$) the term $(z_{j-1} - 2z_j + z_{j+1})$ is replaced by $(z_2 - z_1)$ and for the last by $(z_{n-1} - z_n)$. The stability properties of an oscillator are different for different signs of ε: $\varepsilon = 0$ marks a Hopf bifurcation (Hudspeth, 2014). Reactive coupling refers to a connection between neighbouring oscillators where they are connected by an elastic spring-like structure. In contrast, in dissipative coupling neighbouring oscillators are connected by a shearing force. For example, when two oscillators are connected via a fluid, the motion of one oscillator will produce a fluid motion which stimulates neighbouring oscillators. In equation (1), both reactive and dissipative coupling are present, allowing us to investigate the effects of both types of coupling.

For a single oscillator, without coupling to its neighbours, equation (1) reduces to

$$\dot{z} = (i\omega + \varepsilon)z - b|z|^2 z \qquad (2)$$

Substitution of $z = r(t)e^{i\omega t}$ as a possible solution gives $\dot{r} = \varepsilon r - br^3$, with solution:

$$r(t) = \sqrt{\frac{\varepsilon}{\left(\frac{\varepsilon}{r_0^2} - b\right)e^{-2\varepsilon t} + b}} \qquad (3)$$

with $r_0 = r(0)$; and $r(\infty) = 0$ for $\varepsilon < 0$ and $\sqrt{\frac{\varepsilon}{b}}$ for $\varepsilon > 0$.

Fig. 1 shows solutions $z = r(t)e^{i\omega t}$ of equation (2) for two different parameter combinations. On the quiescent side of the Hopf bifurcation ($\varepsilon < 0$) the oscillation fades out, while for $\varepsilon > 0$ (the self-oscillatory side of the bifurcation) a self-sustaining oscillation builds up.

The set of n coupled differential equations, as given in equation (1), was solved for two values of n with the Mathematica 10 procedure NDSolve, with Method option Automatic, for a time interval sufficiently long to end with a 200 ms long interval with stable oscillations for all oscillators. Initial values for all z_j were 0.01. The natural frequencies $f_j = \omega_j/2\pi$ of the investigated arrays ranged
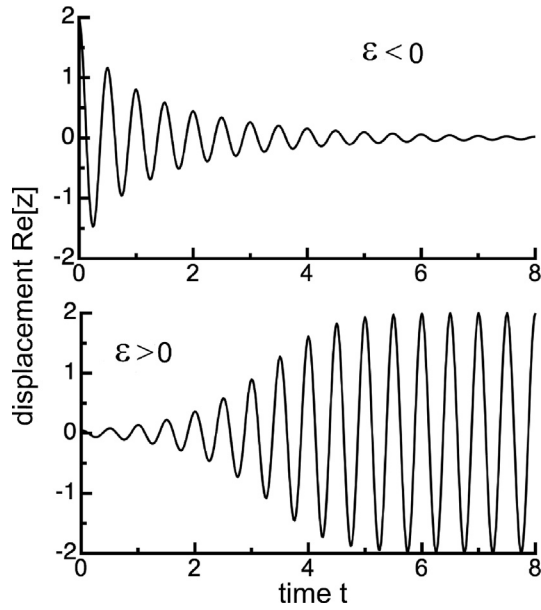
Fig. 1. Solutions of equation (2) for the parameter combinations $\varepsilon = -0.5, r_0 = 2, b = 0.25, \omega = 4\pi$ (upper panel) and for $\varepsilon = 1, r_0 = 0.05, b = 0.25, \omega = 4\pi$ (lower panel).

from 1 to 5 kHz, with an exponential distribution given by

$$f_j = 5^{\frac{j-1}{n-1}} \qquad (4)$$

The array of oscillators is thus tonotopically organized, with a systematic increase of the natural oscillation frequencies along the oscillator array from $j = 1$ to $j = n$. Fourier transforms were calculated for all $x_j(t) = Re[z_j(t)]$ for the 200 ms intervals and their absolute values were taken to obtain amplitude spectra for the individual oscillators. SOAE spectra were modelled as the absolute value of the Fourier transform of the sum of all $x_j(t)$.

3. Application of the model

3.1. Effect of the number of oscillators on the emission spectrum

Previous studies have shown that the oscillators in the array tend to cluster into a small number of oscillation frequencies (Bergevin et al., 2015a; Gelfand et al., 2010; Vilfan and Duke, 2008; Wit et al., 2012; Wit and Bell, 2017). Here, oscillator clustering in an array of 21 and an array of 201 oscillators was compared. For both cases the same set of parameters was chosen: $d_R = 0.07$, $d_I = -1.3$, $\varepsilon_j = b_j = 0.8$ for all j. Fig. 2 shows amplitude spectra for individual oscillators in the two arrays.

To obtain Fig. 3 all $x_j(t)$ for the last 200 ms of the calculated interval were added and the amplitude spectrum was calculated for the sum $\sum_{j=1}^{n} x_j(t)$.

As can be seen in Fig. 2 the amplitude spectrum of an individual oscillator can show more than one peak. Therefore, the frequencies for the plateaus, as shown in Fig. 4, were calculated as the position along the frequency axis of the peak with the largest amplitude in the spectra for the individual oscillators.

Fig. 4 further illustrates the clustering of oscillators in the array. Neighbouring oscillators tend to cluster into common oscillation frequencies, leading to discontinuities between the frequencies of neighbouring clusters. These clusters are visible as plateaus in Fig. 4. Oscillators synchronise at a frequency close to the highest natural frequency within the cluster, which is characteristic for an array with reactive coupling (Vilfan and Duke, 2008).

The two investigated arrays differ tenfold in the number of hair
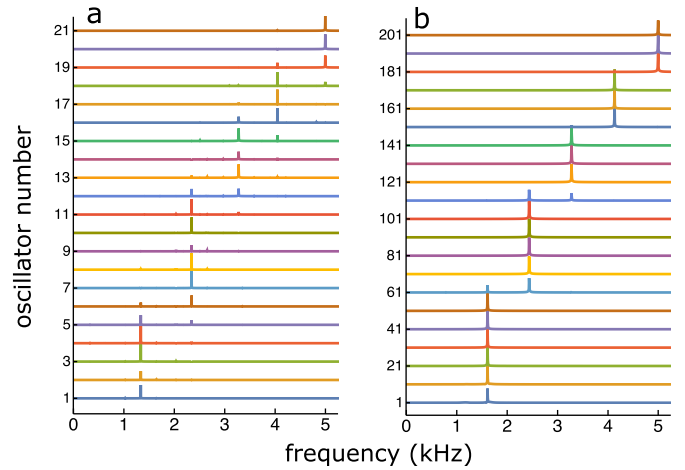

Fig. 2. Calculated amplitude spectra for all oscillators in an array of 21 oscillators (panel a), and for a subset of oscillators in an array of 201 oscillators (panel b).
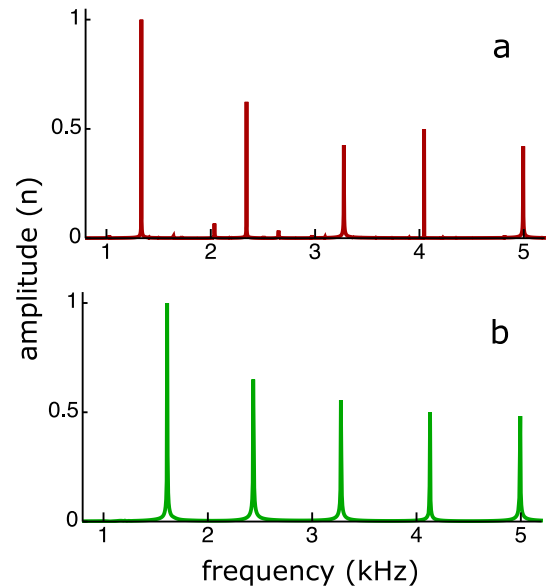

Fig. 3. Amplitude spectrum for the sum of all $x_j(t)$ for an array of 21 oscillators (panel a), or 201 oscillators (panel b).

cells, but their frequency ranges are the same (1–5 kHz). The consequence is that the spacing of the natural frequencies of neighbouring oscillators also differs by a factor 10. Nevertheless, the number of frequency plateaus is the same for both arrays, and correspondingly the number of oscillators per cluster differs by a factor of 10 also. Thus, for the chosen set of oscillator parameters, the number of oscillation clusters does not depend on the number of oscillators in the array. The large 201-oscillator array generates the same number of spectral peaks (Fig. 3) and frequency plateaus (Fig. 4) as the 21-oscillator array. If we assume that these oscillator elements represent hair cells, this result could explain that SOAE frequency spacing in lizards does not relate to papillar size or to the number of hair cells (Manley et al., 2014).

3.2. Effect of the reactive (d_I) and dissipative (d_R) coupling strength on the emission spectrum

Spectra as shown in Figs. 2 and 3 were calculated for an array of 201 oscillators, for a set of d_I-values, ranging from −0.5 to −4 in 70 equal steps. Results are shown in Fig. 5 for 4 values of ε (= ε_j for all
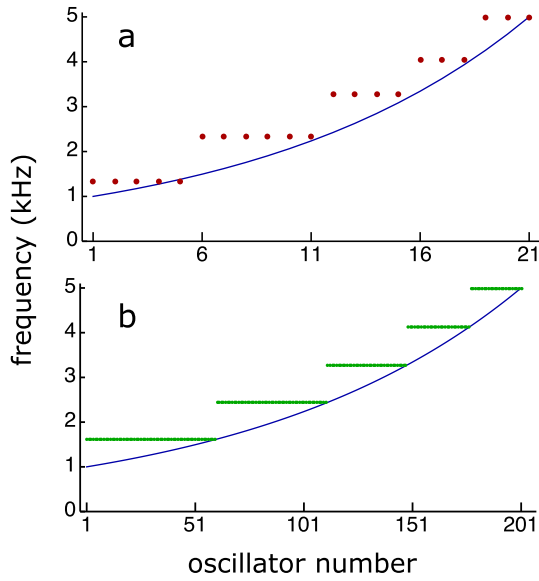
Fig. 4. Red and green dots: frequencies at which oscillators cluster ("frequency plateaus"). Blue lines: natural frequencies of the oscillators. Panel a: array of 21 oscillators. Panel b: array of 201 oscillators. (For interpretation of the references to colour in this figure legend, the reader is referred to the Web version of this article).

j); and in Fig. 6 for 4 values of d_R.

The spectral patterns in Figs. 5 and 6 are relatively robust with respect to the reactive coupling constant d_I and the damping parameter ε. However, when ε becomes very small, the clustering breaks down: see panel 5a. Also no clustering occurs for small (absolute) values of d_I: see the lower traces in all panels in Fig. 5. The striking overall effect is that the reactive coupling constant d_I is the primary parameter to determine whether the oscillators cluster, and in how many frequency plateaus they cluster. The main points that can be taken from Fig. 6 is that some dissipative coupling (parameter d_R) is needed for clustering (panel 6a), but that the patterns of clustering hardly depend on the value of d_R (compare panels 6 b, c, d).

3.3. Roughness

As can be seen in the upper left panel of Fig. 6, no clustering of oscillator frequencies in sharp spectral peaks occurs if dissipative coupling is absent ($d_R = 0$). This is again shown in Fig. 7a. However, if some roughness is introduced in the array of natural frequencies of the oscillators (Fig. 7c), clustering in sharp spectral peaks is again present for certain values of reactive coupling constant d_I (see Fig. 7b). An example of such sharp clustering is shown in Fig. 7d.

3.4. Spectral gaps

For the lizard species Tiliqua rugosa (bobtail skink) the spacing
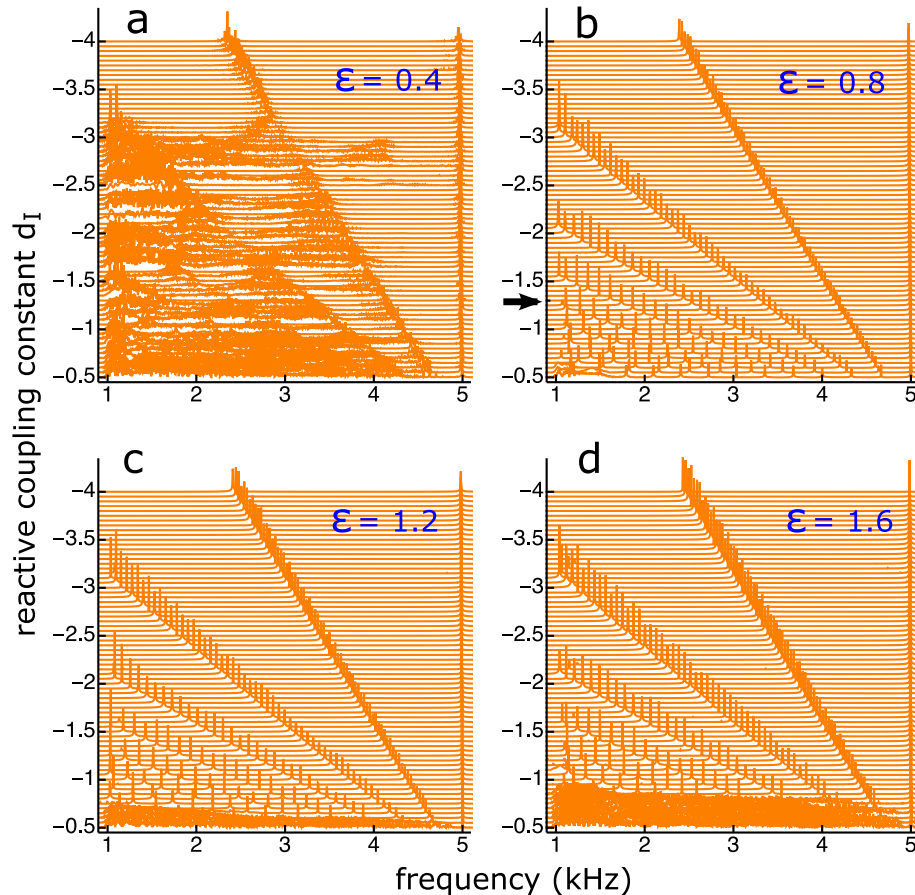
Fig. 5. Waterfall plots of spectra for the sum of all $x_j(t)$, for a range of 71 values of reactive coupling constant d_I, ranging from −0.5 to − 4. The four panels each display results for a different value of effective damping parameter ε. The dissipative coupling constant d_R was equal to 0.07 for all four panels. The arrow in panel b indicates the spectrum for $d_I = −$ 1.3, that is also shown in the lower panel of Fig. 3.

Fig. 6. Same as Fig. 5, except that here the effective damping was fixed at $\varepsilon = 0.8$ and the dissipative coupling constant was different across the 4 panels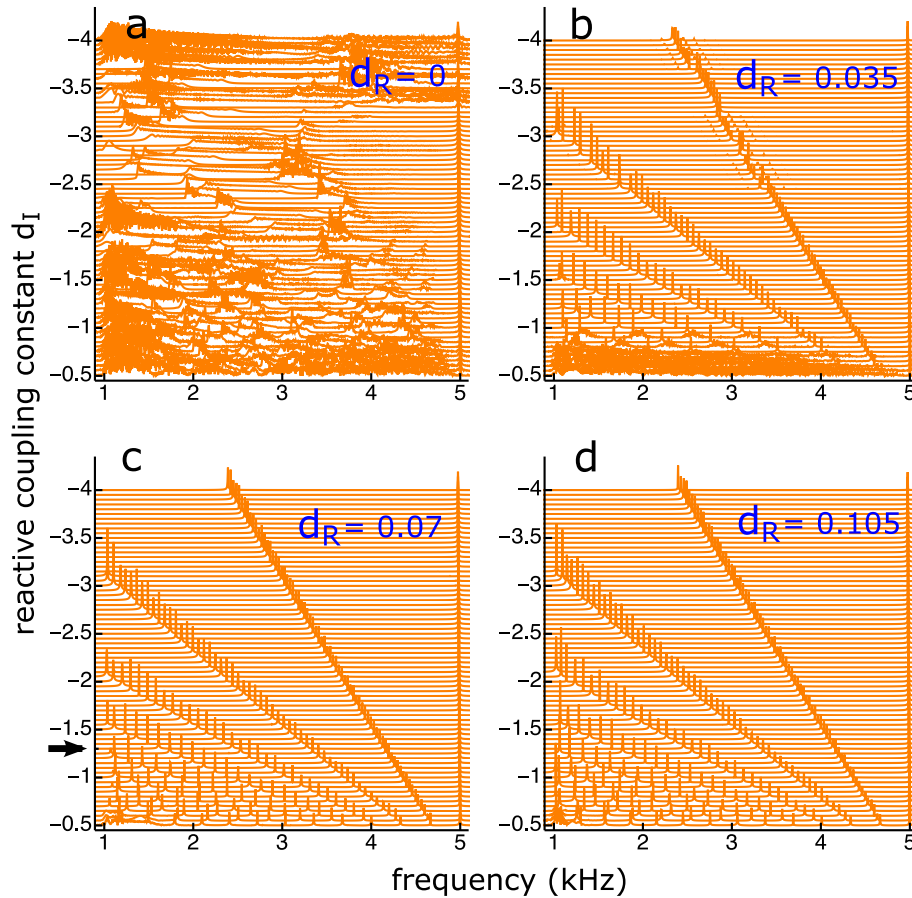. Waterfall plots of spectra for a range of 71 values of reactive coupling constant d_I, ranging from -0.5 to -4, for four values of dissipative coupling constant d_R. The arrow indicates the spectrum for $d_I = -1.3$, that is also shown in the lower panel of Fig. 3.

between SOAE frequencies (spectral gaps) increases with frequency with a factor of about 3 from the lowest to the highest frequency (Köppl and Manley, 1993; Manley et al., 2014). The number of hair cells along the basal (high frequency) segment of the papilla is about 1645 for this species, covering a frequency range from 1 to 5 kHz (Köppl, 1988).

To model this systematically increasing frequency spacing in an array of coupled active oscillators, coupling strength parameter κ_j was added to equation (1):

$$\dot{z}_j = (i\omega_j + \varepsilon_j)z_j + \kappa_j(d_R + id_I)(z_{j-1} - 2z_j + z_{j+1}) - b_j|z_j|^2 z_j \quad (5)$$

Fig. 8 shows the results of the calculation of the oscillator frequencies in an array of 235 oscillators (being 1/7-th of the total number of hair cells, i.e. the number in one row), with natural frequencies $f_j = \omega_j/2\pi$, increasing from 1 to 5 kHz, according to $f_j = 5^{\frac{j-1}{n-1}}$. Coupling strength parameter κ_j increased from 0.4 for $j = 1$ to 1.0 for $j = 235$, following the exponential curve shown in the insert of Fig. 9. Other parameters were: $d_R = 0.08$, $d_I = -0.55$, $\varepsilon_j = b_j = 0.6$ for all j.

The gradual increase of κ_j for increasing j results in a systematic increase in spectral peak spacing from low to high frequencies, as can clearly be seen in Fig. 8b.

The small blue dots in Fig. 9 are SOAE frequency spacings (spectral gaps) for Tiliqua rugosa, as given in Fig. 7a of Köppl and Manley (1993) and in Fig. 1F of Manley et al. (2014). The x-coordinate of these dots is the frequency of the SOAE spectral peak at the

high frequency side of the spectral gap. The solid green line in Fig. 9 is a 10-point moving average of the spacings given by the blue dots. The large red dots mark calculated frequency gaps, being the gaps between the spectral peaks in panel b of Fig. 8 and also the gaps between the frequency plateaus in panel c of the same figure.

The density of hair cells in the basal segment of the papilla of Tiliqua rugosa increases from about 1/100 μm² at the apical (low frequency) end to about 4/100 μm² at the basal (high frequency) end (Köppl, 1988, Fig. 2b). This means that the distance between neighbouring hair cells decreases with about a factor two from apical to basal. This supports the choice of an increasing coupling strength κ_j from the low frequency to the high frequency end of the oscillator array, as shown in the insert of Fig. 9.

3.5. Variability of spectra

For each ear of a lizard with SOAEs, the spectrum of the emitted sound is unique (Köppl and Manley, 1993; Manley et al., 1996), and in general different from the regular spectrum in Fig. 8b.

To account for this uniqueness in human ears, Fruth et al. (2014) introduced, for each individual ear, a different bifurcation parameter profile $\varepsilon(x)$, in their one-dimensional active oscillator array model for the human cochlea. This profile is generated by a spatial version of the stochastic Ornstein-Uhlenbeck process, producing correlation in $\varepsilon(x)$ over a finite correlation length; x being the distance from the stapes along the basilar membrane. According to Fruth et al. (2014), correlation of irregularities along the cochlear partition could be a result of irregularities in the developmental process of the cochlea,
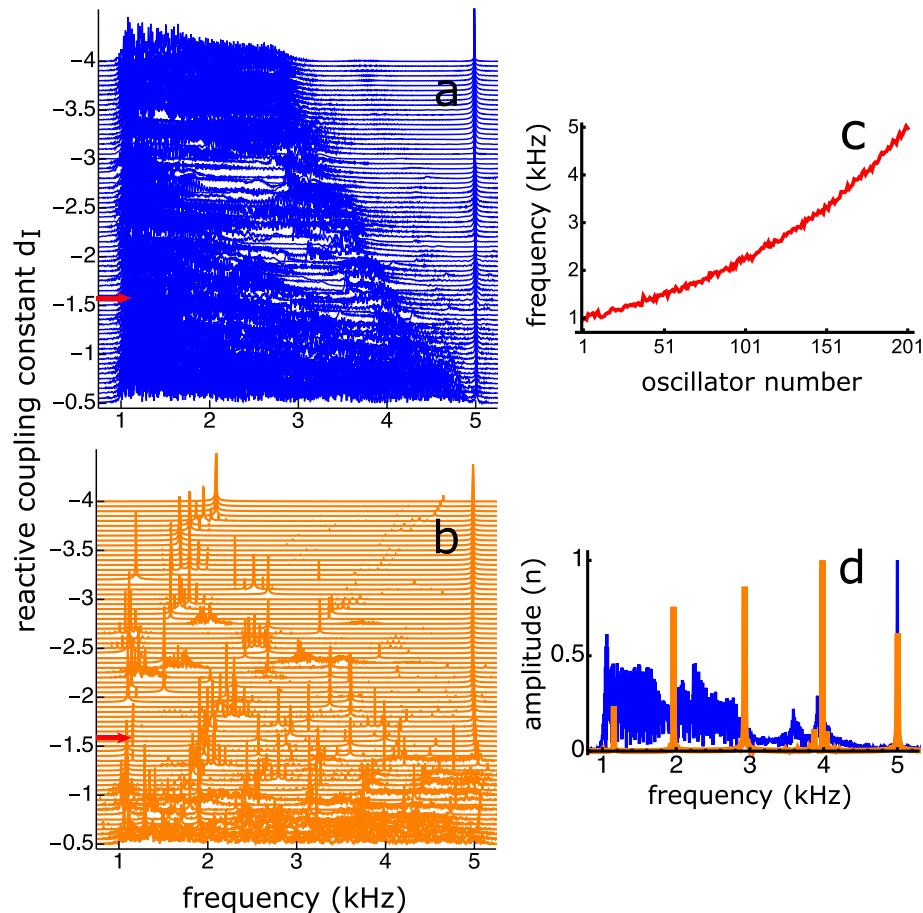
Fig. 7. Left panels: Waterfall plots of spectra for a range of 71 values of reactive coupling constant d_I, for dissipative coupling constant $d_R = 0$ and $\varepsilon = 1.5$. Panel a: For a smooth array of natural oscillator frequencies. Panel b: After the introduction of irregularities in this array, with a normal distribution and a standard deviation of 40 Hz, as shown in panel c. Panel d: Spectra for $d_I = -1.6$, indicated with small red arrows in the left panels. Blue spectrum: from panel a. Orange spectrum: from panel b. (For interpretation of the references to colour in this figure legend, the reader is referred to the Web version of this article).

as suggested earlier by Manley (1983).To investigate the influence of an irregular ε_j profile on the shape of a calculated amplitude spectrum, we repeated the calculations that produced the results as shown in Fig. 8, but now for an irregular profile of ε, instead of a constant value (in Fig. 8: $\varepsilon_j = 0.6$ for all j). The other parameters were the same as in Fig. 8. The ε-profile was generated with the *Mathematica* procedure *OrnsteinUhlenbeckProcess*[μ, σ, θ, ε_0], with long term mean $\mu = 0.6$, volatility $\sigma = 0.6$, mean reversion speed $\theta = 0.2$ and initial value $\varepsilon_0 = 0.6$. Results are shown in Fig. 10, in separate panels for three different ε-profiles.

Van Dijk and Manley (2013) report that lizard SOAEs show two characteristics that have not been described in humans: (1) spectra with emission peaks on top of broad plateaus, and (2) spectral peaks with the characteristics of narrow band noise.Such broad plateaus, with a few pronouncing spectral peaks, are indicated with arrows in Fig. 10.

3.6. Noise

An important effect of subjecting the oscillators in an array of coupled oscillators to noise is that spectral peaks are broadened (Vilfan and Duke, 2008; Jülicher et al., 2009; Gelfand et al., 2010), resulting in peak widths as measured in real lizard ears (Köppl and Manley, 1993, Fig. 5). We explored this phenomenon by adding noise terms to the set of equation (1).

As a first illustration Fig. 11 gives the spectrum for the sum of all

$x_j(t)$ for an array of 21 oscillators, with the same ω_j as for the calculation of Figs. 2a, 3a and 4a. For this purpose the term $\zeta_j(t)$, being white Gaussian noise with mean 0 and standard deviation 1, was added to the right side of equation (1). Just like Vilfan and Duke (2008) we assumed, for the sake of simplicity and realistic calculation times, that all oscillators were subjected to the same noise force. Other parameters were: $d_R = 0.05$, $d_I = -4$, $b_j = 1$ for all j. It can be seen in Fig. 11 that adding noise not only broadens the spectral peaks. It also introduces extra (low frequency) peaks.Adding noise to equation (1) increased calculation time by more than a factor 200. For this reason the number of oscillators was at first limited to 21.

After this the calculations resulting in Fig. 11 were repeated, but now for an array of 201 oscillators, instead of 21. Parameters were: $d_R = 0.07$, $d_I = -1.3$, b = 1.0. The sum $s_k(t)$ of all 201 $x_j(t)$ was calculated for an interval of 250 ms. This calculation was repeated 10 times for a randomly generated Gaussian noise force each time, with standard deviation 0.7 and being the same for all oscillators. The epsilon-profile, as shown in Fig. 12, was the same for all 10 calculations. It was generated as described above for Fig. 10.

Amplitude spectra were calculated for all 10 $s_k(t)$, and averaged. The average amplitude spectrum is shown in Fig. 13. As for the array with 21 oscillators, the main effect of the noise was a broadening of the spectral peaks and the generation of background noise along the whole frequency axis.

After this all 10 $s_k(t)$ were joined, giving a time-signal s(t) with a duration of 2.5 s. Signal s(t) was then filtered with a second order
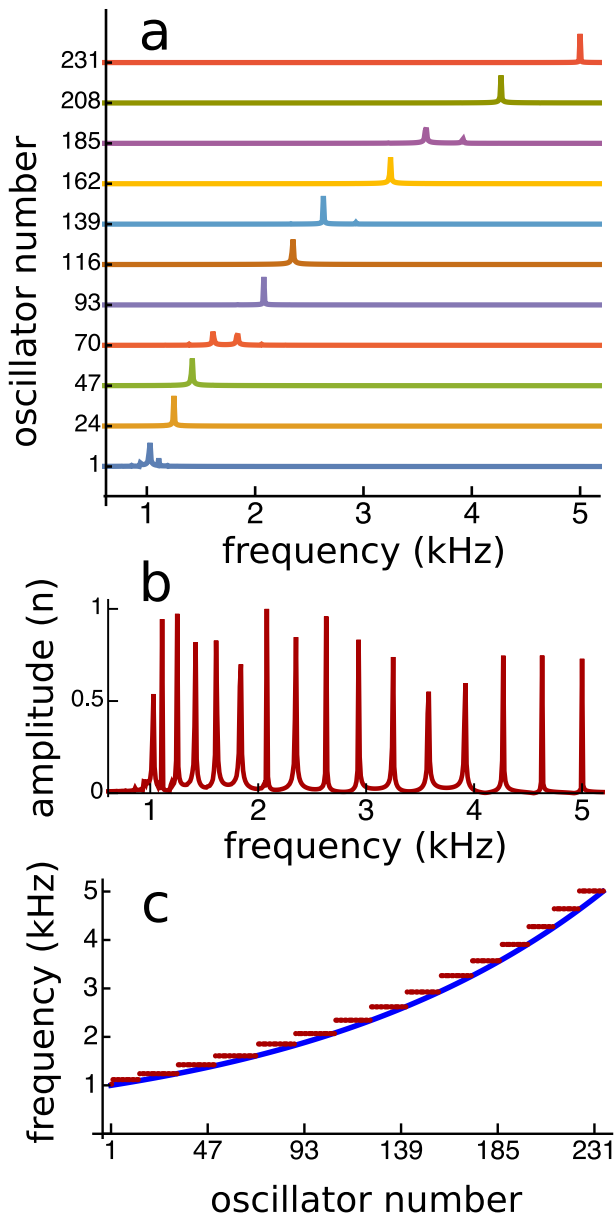
Fig. 8. Compilation of the figures shown as Figs. 2–4; now for coupling strength κ_j increasing with oscillator number j, as shown in the insert of Fig. 9.

Fig. 9. Small blue dots: SOAE frequency spacings in Tiliqua rugosa. Solid green line: 10-point moving average of these frequency spacings. Large red dots: gaps between the calculated frequency plateaus in Fig. 8c. Insert in upper left corner: coupling strength parameter κ_j as function of oscillator number j. (For interpretation of the references to colour in this figure legend, the reader is referred to the Web version of this article).

owl and lizard ears.

The calculations producing Figs. 13 and 14 were repeated, again for an array of 201 oscillators, for the same set of parameters ($d_R = 0.07$, $d_I = -1.3$, b = 1.0.), but now for a constant value 0.8 for ε_j, for all j, instead of an irregular profile. Standard deviation of the noise was 0.5. The resulting spectrum is shown in Fig. 15.

In contrast with the spectrum in Fig. 13 (for an irregular ε_j-profile) the spectral peaks in Fig. 15 become systematically narrower from low to high frequency. The consequence of this is illustrated in Fig. 16: the ring-shaped elevation surrounding the center of a histogram becomes systematically more prominent from low to high frequencies.

Comparable different 3D shapes (ring only, ring with central peak, central peak only), as shown in Figs. 14 and 16, are obtained for probability density distributions for sinusoidally driven single noisy Hopf oscillators, for different values of the parameter controlling the criticality of the oscillator (Ó Maoiléidigh, 2018). (The question as to why the 3D-histograms for single noisy Hopf oscillators resemble those for an array of coupled oscillators, subjected to noise, is beyond the scope of the present paper.)

4. Discussion

This paper explores the behaviour of a model of coupled self-sustained oscillators, originally developed by Vilfan and Duke (2008), in order to describe spectra of spontaneous otoacoustic emissions in lizards. The principle result is that neighbouring oscillators tend to synchronise to each other, thus collectively generating a single oscillation frequency. The entire array of oscillators consequently generates a limited number of discrete oscillation frequencies, which are proposed to model spontaneous otoacoustic emission from the lizard ear.

In all simulations, the natural frequencies of the oscillators were fixed to range from 1 to 5 kHz. Nevertheless, a range of behaviours could be simulated by manipulating the coupling between the oscillators, the resistance of the oscillators, and the number of oscillators in the model. A remarkable result is that the number of peaks in the simulated spectra does not critically depend on the number of oscillators in the model (Figs. 2–4). This corresponds to the observation that lizard ears with only few hair cells, e.g., the iguanid Anolis, produce emission spectra with numerous peaks (Manley and Gallo, 1997), similar to species with many more hair cells (e.g. geckos, Manley et al., 1996; skinks, Köppl and Manley, 1993).

Butterworth filter with a full width of 120 Hz and a central frequency equal to the frequency of one of the spectral peaks (see Fig. 13), resulting in the narrow-band filtered signal f(t). Envelope r(t) and phase $\varphi(t)$ of f(t) were calculated with the Hilbert-transform and combined to give the complex array z(t) = r(t) $e^{i\varphi(t)}$. The real and imaginary parts of z(t) were combined in a 2-dimensional array, and for this array a three dimensional (3D) histogram was calculated. (As elucidated in the Appendix). This process was repeated for all 6 spectral peaks from left to right. The result is shown in Fig. 14 in this order.

The 3D-histograms in Fig. 14 are a measure for the stability of the amplitude of the band-pass filtered signal. They were, as a generalisation of the Bialek-Wit histogram (Bialek and Wit, 1984, Fig. 2), introduced by Shera (Shera, 2003: Fig. 7), and can be compared with the histograms in Fig. S3 in the supporting information of Bergevin et al. (2015a), and in Fig. 1 of Bergevin and Salerno (2014), being histograms for SOAEs measured in human,
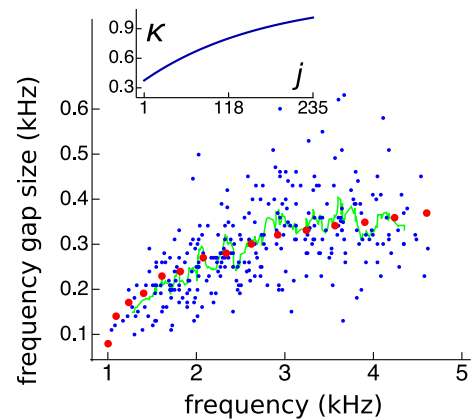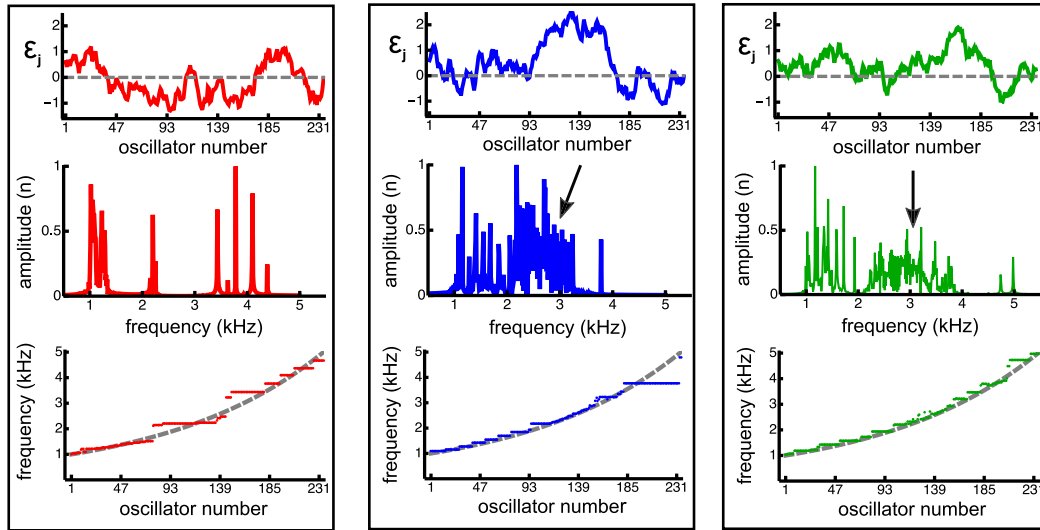
Fig. 10. Clustering behaviour in an array of 235 oscillators for three different profiles (upper row) of effective damping parameter ε_j. (Oscillator j is active if $\varepsilon_j > 0$, and passive if $\varepsilon_j < 0$). Middle row: Calculated amplitude spectrum for the sum of all $x_j(t)$ for an array of 235 oscillators, as in Fig. 8b. Lower row: Position along the frequency axis of the peak with the largest amplitude in the spectra for the individual oscillators, as in Figs. 4 and 8c. The arrows indicate spectral plateaus.
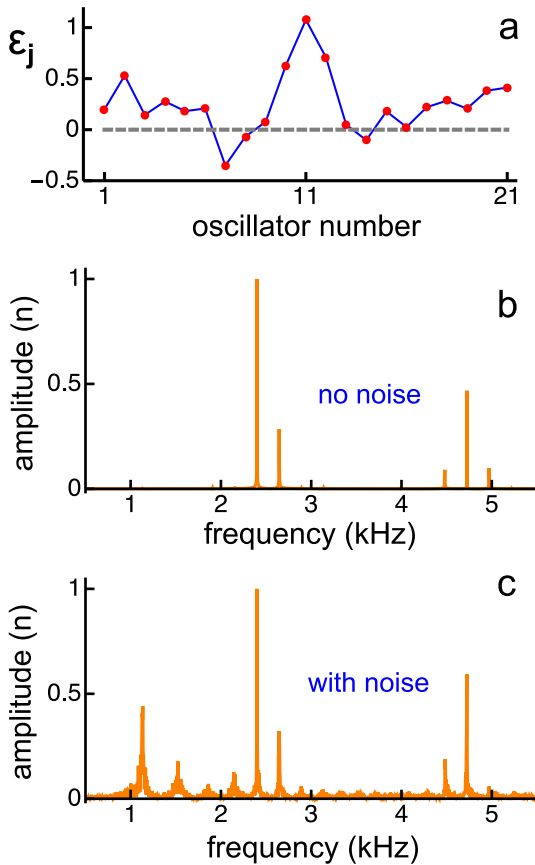

Fig. 12. Profile of effective damping parameter ε_j for an array of 201 oscillators.

Fig. 13. Orange line: Amplitude spectrum for an array of 201 oscillators, all subject to Gaussian noise, for an ε_j-profile as shown in Fig. 12. The spectrum is the average of the amplitude spectra for 10 separately calculated time signals, each with a duration of 0.25 s. Blue dashed line: Typical profile of the filter used to isolate the signals corresponding to individual spectral peaks. These filtered signals were used to generate the histograms in Fig. 14. (For interpretation of the references to colour in this figure legend, the reader is referred to the Web version of this article).

Fig. 11. Panel a: profile of effective damping parameter ε_j. Lower panels: spectra for the sum of all $x_j(t)$, for 21 oscillators, without (panel b) and with noise (panel c).

spectrum. Although the current model was intended to model lizard SOAE, this is also reminiscent of spectra in the frog inner ear. SOAEs from the frog amphibian papilla have the highest emission frequency typically at the upper edge, or even above, the highest neural characteristic frequency of that organ (see Fig. 7.2 in Manley and van Dijk, 2008). The model would suggest that the high-frequency portion of the amphibian papilla clusters to produce an SOAE peak at the upper edge of the frequency response range of that papilla.

Comparison of Fig. 5b, c and d reveals that the spectral patterns into which the oscillators cluster hardly depend on the effective damping of the oscillators (parameter ε), for a fixed small value of the resistive damping parameter d_R. The same holds for the influence of d_R (if it is different from 0), for a fixed value of ε, as a comparison of Fig. 6b, c and d shows. However, the spacing of the spectral peaks critically depends on the strength of the reactive

Moreover, oscillators tend to gather to the highest frequency in a cluster (Fig. 4), regardless of the number of oscillators. This is a property of oscillators with mainly reactive coupling (Vilfan and Duke, 2008, Fig. 3B). Consequently, the highest frequency in a recorded emission spectrum may reflect the upper limit of characteristic frequencies of the hair cells contributing to the SOAE
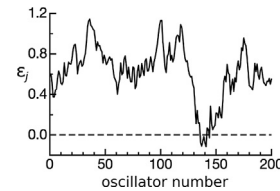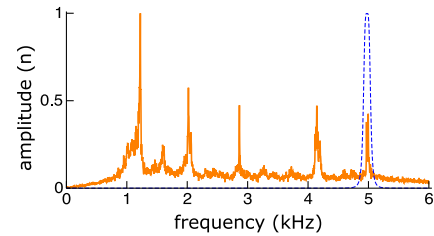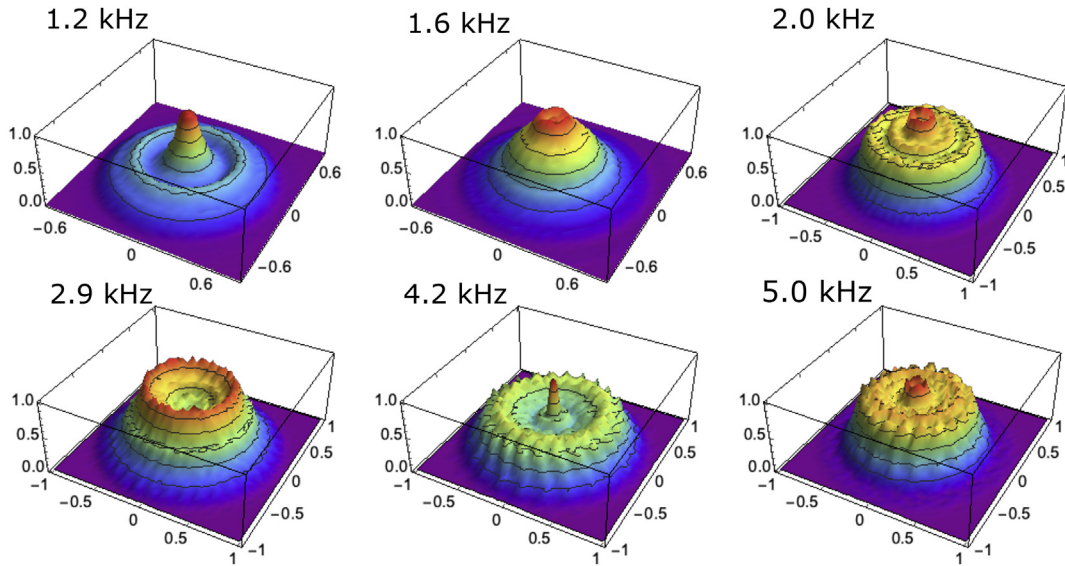
Fig. 14. 3D histograms for the spectral peaks in Fig. 13, calculated as described in the text and the Appendix. Normalised histogram bin values are in the vertical direction.
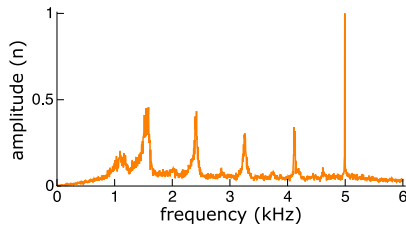

Fig. 15. Amplitude spectrum for an array of 201 oscillators, all subject to Gaussian noise, for $\varepsilon_j = 0.8$ for all j.The spectrum is the average of the amplitude spectra for 10 separately calculated time signals, each with a duration of 0.25 s.

(spring-like) coupling between the oscillators (parameter d_I), as can be seen in Fig. 17, being details of Fig. 5b (or Fig. 6c). The peaks in a single spectrum of Fig. 17 are (almost) equidistant. The distance between two neighbouring peaks increases linearly from 0.33 to 2.6 kHz, for $|d_I|$ increasing from 0.5 to 4.0. The number of oscillators

(total 201) that cluster at a single frequency increases roughly by a factor 10 for this d_I-range.

In lizard species with so-called free-standing hair cells, such as Anolis, the spacing between SOAE peaks is relatively small as compared to species where the hair cells are covered by a tectorial membrane (such as the monitor lizard Varanus, Manley, 2004). A large spacing correlates, of course, with the presence of fewer peaks. The lack of a tectorial membrane presumably corresponds to weak reactive coupling. Thus, consistent with the model results, weak coupling in free-standing hair cells (small d_I in Figs. 5 and 6) corresponds to narrow SOAE peak spacing, as compared to stronger coupling due to a continuous tectorial membrane covering the hair cells.

Besides the strength and nature of the coupling between neighbouring oscillators, irregularities in the tonotopic gradient of the array also contribute to the formation of distinct oscillation peaks in the composite model spectrum (Fig. 7). While the absence of dissipative coupling results in a spectrum without clearly distinguishable
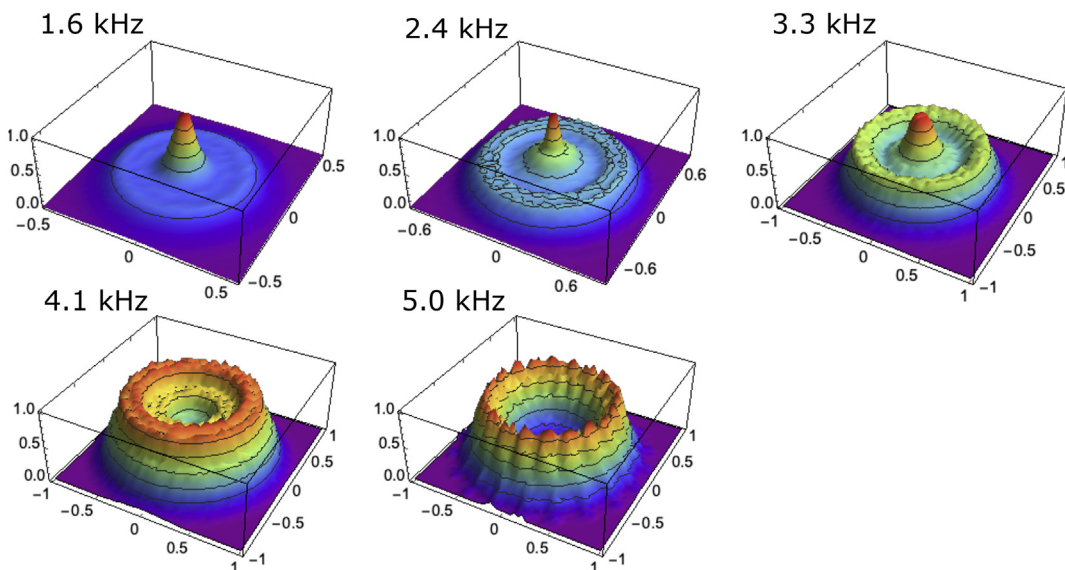

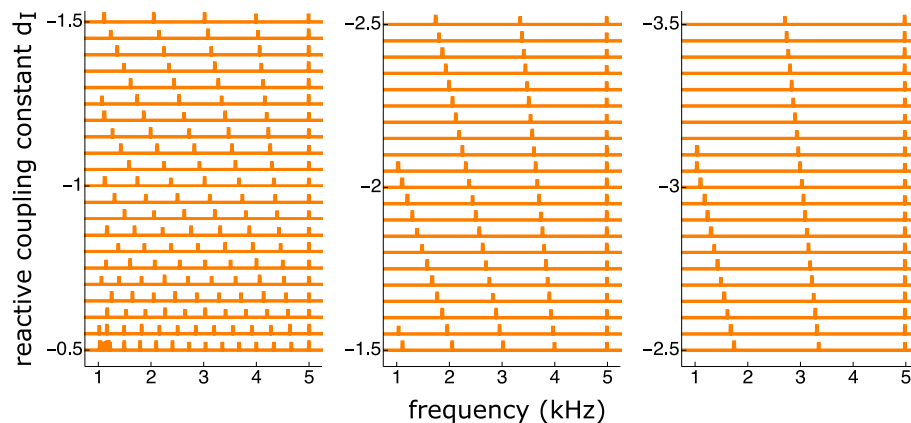**Fig. 16.** 3D-histograms for the spectral peaks in Fig. 15.

Fig. 17. Waterfall plots of spectra for the sum of all $x_j(t)$, for 3 ranges of reactive coupling constant d_I, being details of Fig. 5b (or Fig. 6c). (All spectral peaks have been given the same amplitude for clarity).

peaks (Fig. 7a), the introduction of irregularities causes distinct peaks in the summed spectrum. That the introduction of roughness, in the absence of dissipative coupling, can cause frequency clustering was already noticed by Epp et al. (2014). And in addition, Osipov and Sushchik (1998) showed that synchronisation in an array of oscillators occurs for a broader range of parameters in a randomly formed array than for regularly arranged oscillators, with their natural frequencies varying monotonically along the array.

In all initial simulations, the spectral peaks produced by the model are narrow, indicating that highly stable oscillations are generated. This is in contrast with observed data in lizards, where the spectral width of SOAE peaks varies. In the Bobtail skink, e.g., the 3 dB peak bandwidth varies from 25 to more than 200 Hz, correlating inversely with the peak amplitudes (Köppl and Manley, 1993). Introducing noise into the individual oscillators of the model created such more realistic spectra (Fig. 13), as already shown by Vilfan and Duke (2008, Fig. 5), who simultaneously introduced irregularities and noise into their model. Comparably, instabilities in an active filter can model the statistical properties of human SOAEs (Bialek and Wit, 1984; Van Dijk and Wit, 1990).

All calculations above were carried out using an exponential relation between oscillator number and its natural frequency; see equation (4). This choice affects, among other things, the spacing of the spectral peaks: spacing increases with increasing natural frequency (see Figs. 8 and 9). If the relation between oscillator number and natural frequency is, instead, linear, the spacing between peaks in modeled SOAE spectra is also linear (Vilfan and Duke, 2008, Fig. 2). This is more or less the case in the barn owl's inner ear, where the place-frequency map of the papilla includes a foveal region centered in the owl's basal half papilla (Köppl et al., 1993, Fig. 8). This corresponds to the unique and essentially equal spacing of SOAE in the barn owl across the frequency range (Bergevin et al., 2015b).

The coupling between the oscillators in the model used here (Vilfan and Duke, 2008) is nearest-neighbour coupling: each oscillator in the array is coupled to both its neighbours only. In many models for the mammalian cochlea, coupling between the oscillatory elements is through the inner ear fluid only, so that each oscillator is coupled to all other oscillators. A rather recent elaboration of the latter is the model of (Elliott et al. 2011; Elliott and Ni, 2018). Fruth et al. (2014) combined fluid- and nearest-neighbour coupling in their model, that describes the statistics of human SOAEs.

Apparently, assuming nearest-neighbour coupling only is sufficient to describe many aspects of SOAEs in lizards, as the present work shows; as well as characteristics of human SOAEs (Wit and van Dijk, 2012).

5. Conclusion

A model of coupled oscillators accounts for all characteristic properties of SOAEs in lizard. The reactive coupling strength between neighbouring oscillators determines to a large extent the details of the simulated spectra. Resistive coupling, oscillator strength and the number of oscillators are of lesser importance. Lizard species differ from each other with respect to number of hair cells, tectorial coupling between hair cells, and SOAE characteristics (Manley, 1997). The results of the current paper provide a basic understanding of these differences in SOAE characteristics.

Appendix

All signals, for which histograms - as shown in Figs. 14 and 16 - were calculated, are one-dimensional arrays $\mathbf{x} = \{x_1, x_2, \ldots, x_n\}, n = 250,000$. The arrays were normalised by dividing them by their maximum value. By Hilbert transformation of $\mathbf{x}$ an array of complex numbers $\mathbf{z}$ was obtained.

In the following, the procedure to obtain the 3.3 kHz histogram in Fig. 16 is illustrated.

One thousand complex numbers, obtained by taking each 250-th element of $\mathbf{z}$, are plotted in the complex plane, giving Fig. 18A. Figs. 18B and C are, respectively, a normalised 2D-histogram and a normalised 3D-histogram for all 250,000 z_j, for a bin size of 0.04 × 0.04. Fig. 18C is the same as the 3.3 kHz histogram in Fig. 16. The Bialek-Wit histogram in Fig. 18D is "simply" obtained as the distribution of all x_j, for a bin width of 0.04.

In polar coordinates the positions of the z_j in the complex plane are given by $r_j = Abs[z_j]$ and $\varphi_j = Arg[z_j]$. Fig. 18E gives the histogram for all r_j, again for a bin width of 0.04.

As can be seen in Fig. 18A, B and C, there is no relevant information in the φ_j; each value from 0 to 2π is equally possible for φ_j. The conclusion must then be that all relevant information is in the r_j. As can be seen in Fig. 18E, most r_j values are in the bin with central value 0.62, while the histograms in Fig. 18B and C have their maximum around the origin of the complex plane. The almost 30,000 values in the bin with central value 0.62 are points in the complex plane in a ring around the origin, with a width of 0.04 and a central radius of 0.62. The area of this ring is proportional to its radius. The density of the points in the ring is obtained by dividing the number of points inside the ring by its area. So, by dividing each bin frequency in Fig. 18E by the bin's central value, the density histogram of Fig. 18F is obtained. Rotating this histogram around its vertical axis gives a 3D figure with the approximate shape of Fig. 18C.
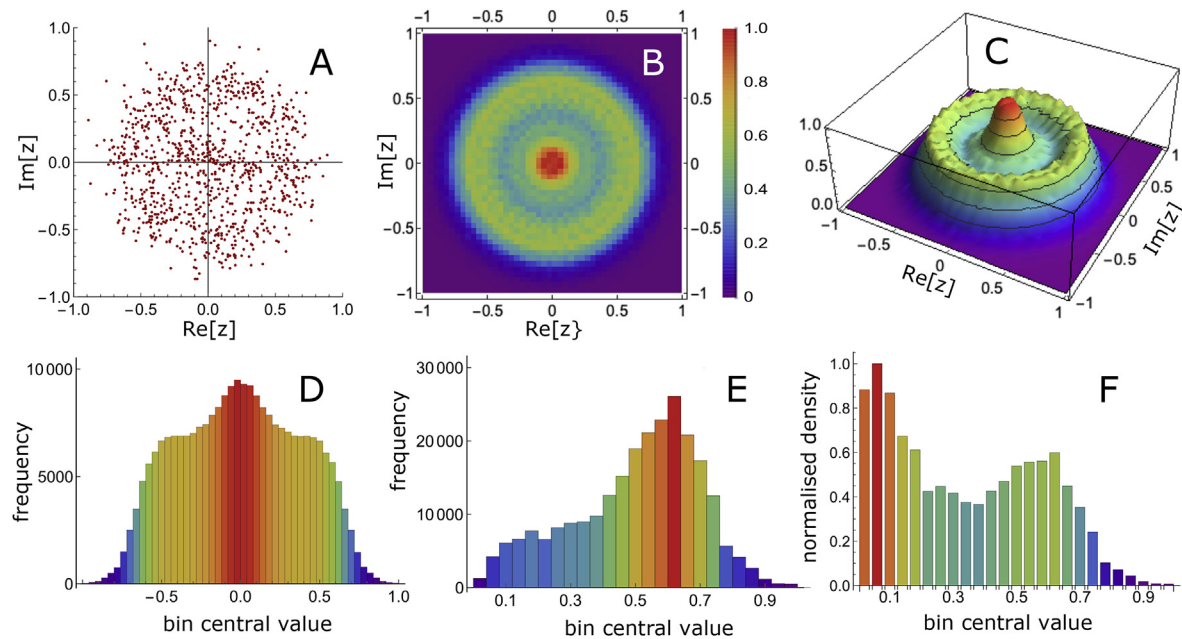
Fig. 18. A. Subgroup of all z_j (see text), plotted in the complex plane. B. 2D - histogram for all z_j. C. 3D - histogram for all z_j. D. Bialek-Wit histogram for all x_j (see text). E. Histogram for all $Abs[z_j]$. F. Histogram for the density distribution in the complex plane for all z_j.

Appendix A. Supplementary data

Supplementary data to this article can be found online at https://doi.org/10.1016/j.heares.2019.107840.

References

Bialek, W., Wit, H.P., 1984. Quantum limits to oscillator stability: theory and experiments on acoustic emissions from the human ear. Phys. Rev. Lett. 104A, 173–178.

Bergevin, C., Salerno, A., 2014. Dynamics of spontaneous otoacoustic emissions. In: Proceedings of the 12th International Workshop "Mechanics of Hearing" in Attica, Greece.

Bergevin, C., Manley, G.A., Köppl, C., 2015a. Salient features of otoacoustic emissions are common across tetrapod groups and suggest shared properties of generation mechanisms. Proc. Natl. Acad. Sci. doi: 10.1073/pnas. 1418569112.

Bergevin, C., Manley, G.A., Köppl, C., 2015b. Otoacoustic interrelationships of the barn owl. In: Karavitaki, K.D., Corey, D.P. (Eds.), Mechanics of Hearing: Protein to Perception. American Institute of Physics, Melville, NY. https://doi.org/10.1063/1.4939409. AIP Conference Proceedings 1703, 090011/1-5.

Burns, E.M., 2009. Long-term stability of spontaneous otoacoustic emissions. J. Acoust. Soc. Am. 125, 3166–3176.

Daido, H., 1999. Complexity and scaling of frequency plateaus in chains of coupled nonlinear oscillators. Prog. Theor. Phys. 102, 197–202.

Elliott, S.J., Lineton, B., Ni, G., 2011. Fluid coupling in a discrete model of cochlear mechanics. J. Acoust. Soc. Am. 130, 1441–1451.

Elliott, S.J., Ni, G., 2018. An elemental approach to modelling the mechanics of the cochlea. Hear. Res. 360, 14–24.

Epp, B., Wit, H.P., van Dijk, P., 2014. Clustering of cochlear oscillations in frequency plateaus as a tool to investigate SOAE generation. In: Proceedings of the 12th International Workshop "Mechanics of Hearing" in Attica, Greece.

Ermentrout, G.B., Kopell, N., 1984. Frequency plateaus in a chain of weakly couples oscillators. SIAM J. Math. Anal. 15, 215–237.

Fruth, F., Jülicher, F., Lindner, B., 2014. An active oscillator model describes the statistics of spontaneous otoacoustic emissions. Biophys. J. 107, 815–824.

Gelfand, M., Piro, O., Magnasco, M.O., Hudspeth, A.J., 2010. Interactions between hair cells shape spontaneous otoacoustic emissions in a model of the Tokay Gecko's cochlea. PLoS One 5 (6), e11116. https://doi.org/10.1371/journal.pone.0011116.

Hudspeth, A.J., 1997. Mechanical amplification of stimuli by hair cells. Curr. Opin. Neurobiol. 7, 480–486.

Hudspeth, A.J., 2014. Integrating the active process of hair cells with cochlear function. Nat. Rev. Neurosci. 15, 1–15.

Jülicher, F., Dierkes, K., Lindner, B., Prost, J., Martin, P., 2009. Spontaneous movements and linear response of a noisy oscillator. Eur. Phys. J. E. https://doi.org/10.1140/epje/i2009-10487-5.

Köppl, C., 1988. Morphology of the basilar papilla of the bobtail lizard Tiliqua

rugosa. Hear. Res. 35, 57–169.

Köppl, C., 1995. Otoacoustic emissions as an indicator for active cochlear mechanics: a primitive property of vertebrate auditory organs. In: Manley, G.A., Klump, G.M., Köppl, C., Fastl, H., Oeckinghaus, H. (Eds.), Advances in Hearing Research. World Scientific Publishing, Singapore, pp. 207–218.

Köppl, C., Gleich, O., Manley, G.A., 1993. An auditory fovea in the barn owl cochlea. J. Comp. Physiol. 171, 695–704.

Köppl, C., Manley, G.A., 1993. Spontaneous otoacoustic emissions in the bobtail lizard. I: general characteristics. Hear. Res. 71, 157–169.

Köppl, C., Manley, G.A., 1994. Spontaneous otoacoustic emissions in the bobtail lizard. II: interactions with external tones. Hear. Res. 72, 159–170.

Manley, G.A., 1983. Frequency spacing of acoustic emissions: a possible explanation. In: Webster, W.R., Aitkan, L.M. (Eds.), Mechanisms of Hearing, Melbourne, Australia, pp. 36–39.

Manley, G.A., 1997. Diversity in hearing-organ structure and the characteristics of spontaneous otoacoustic emissions in lizards. In: Lewis, E.R., Long, G.R., Lyon, R.F., Narins, P.M., Steele, C.R. (Eds.), Diversity in Auditory Mechanics. World Scientific Publishing, Singapore, pp. 32–38.

Manley, G.A., 2001. Evidence for an active process and a cochlear amplifier in non-mammals. J. Neurophysiol. 86, 541–549.

Manley, G.A., 2002. Evolution of structure and function of the hearing organ of lizards. J. Neurobiol. 53, 202–211.

Manley, G.A., 2004. Spontaneous otoacoustic emissions in monitor lizards. Hear. Res. 189, 41–57.

Manley, G.A., 2011. Lizard auditory papillae: an evolutionary kaleidoscope. Hear. Res. 273, 59–64.

Manley, G.A., Köppl, C., 1994. Spontaneous otoacoustic emissions in the bobtail lizard. III: temperature effects. Hear. Res. 72, 171–180.

Manley, G.A., Gallo, L., Köppl, C., 1996. Spontaneous otoacoustic emissions in two gecko species, Gekko gecko and Eublepharis macularius. J. Acoust. Soc. Am. 99, 1588–1603.

Manley, G.A., Gallo, L., 1997. Otoacoustic emissions, hair cells and myosin motors. J. Acoust. Soc. Am. 102, 1049–1055.

Manley, G.A., Kirk, D., Köppl, C., Yates, G.K., 2001. In-vivo evidence for a cochlear amplifier in the hair-cell bundle of lizards. Proc. Natl. Acad. Sci. U.S.A. 98, 2826–2831.

Manley, G.A., Köppl, C., 2008. What have lizard ears taught us about auditory physiology? Hear. Res. 238, 3–11.

Manley, G.A., van Dijk, P., 2008. Otoacoustic emissions in amphibians, lepidosaurs and archosaurs. In: Manley, G.A., Fay, R.R., Popper, A. (Eds.), Active Processes and Otoacoustic Emissions in Hearing; Springer Handbook of Auditory Research, vol. 30. Springer Science + Business Media, LLC, New York, pp. 211–260.

Manley, G.A., Köppl, C., Bergevin, C., 2014. Common substructure in otoacoustic emission spectra of land vertebrates. In: Proceedings of the 12th International Workshop "Mechanics of Hearing" in Attica, Greece.

Miller, M.R., 1966. The cochlear duct of lizards. Proc. Calif. Acad. Sci. 33, 255–359.

Ó Maoiléidigh, D., 2018. Multiple mechanisms for stochastic resonance are inherent to sinusoidally driven noisy Hopf oscillators. Phys. Rev. E 97, 022226.

Osipov, G.V., Sushchik, M.M., 1998. Synchronized clusters and multistability in arrays of oscillators with different natural frequencies. Phys. Rev. E 58, 7198—7207.

Shera, C.A., 2003. Mammalian spontaneous otoacoustic emissions are amplitude-stabilized cochlear standing waves. J. Acoust. Soc. Am. 114, 244—262.

Shera, C.A., Guinan, J.J., 2003. Stimulus-frequency group delay: A test of coherent reflection filtering and a window on cochlear tuning. J. Acoust. Soc. Am. 113, 2762—2772.

Taschenberger, G., Manley, G.A., 1997. Spontaneous otoacoustic emissions in the barn owl. Hear. Res. 110, 61—76.

Van Dijk, P., Wit, H.P., 1990. Amplitude and frequency fluctuations of spontaneous otoacoustic emissions. J. Acoust. Soc. Am. 88, 1779—1793.

Van Dijk, P., Manley, G.A., 2013. The effect op air pressure on spontaneous otoacoustic emissions of lizards. J. Ass. Res. Otolaryngol. 14, 309—319.

Vilfan, A., Duke, T., 2008. Frequency clustering in spontaneous otoacoustic emissions from a lizard's ear. Biophys. J. 95, 4622—4630.

Wever, E.G., 1978. The Reptile Ear. Princeton Univ Press, Princeton.

Wit, H.P., van Dijk, P., 2012. Are human spontaneous otoacoustic emissions generated by a chain of coupled nonlinear oscillators? J. Acoust. Soc. Am. 132, 918—926.

Wit, H.P., van Dijk, P., Manley, G.A., 2012. A model for the relation between stimulus frequency and spontaneous otoacoustic emissions in lizard papillae. J. Acoust. Soc. Am. 132, 3273—3279.

Wit, H.P., Bell, A., 2017. Clusters in a chain of coupled oscillators behave like a single oscillator: relevance to spontaneous otoacoustic emissions from human ears. J. Hear. Sci. 7, 19—26.